Fire Technology

Manufactured in The United States
https://doi.org/10.1007/s10694-022-01258-7

Multi-degree-of-freedom Hybrid Fire Testing of a Column in a Non-linear Environment

Elke Mergny * *and Jean-Marc Franssen, Urban and Environmental Engineering (UEE), Liège University, Liège, Belgium*

Received: 30 October 2021/**Accepted:** 12 April 2022

Abstract. Hybrid fire testing is a testing method for structures on fire based on a substructuring method. A complete structure is divided in two substructures, one in a fire test laboratory (physical substructure), and one numerically simulated (numerical substructure). In fire engineering, some hybrid fire tests have been successfully performed in the last decades, but as the method is still in its infancy, these hybrid tests were limited to one-degree-of-freedom tests. The paper presents the first successful multi-degree-of-freedom hybrid test performed in fire engineering. The physical substructure is a steel column with an axial displacement and rotations at the ends controlled by electric jacks. The numerical substructure is a non-linear 2D plane frame structure modelled in SAFIR®. The equations of the algorithm, the experimental setup, the testing process, and the results are presented.

Keywords: Hybrid fire testing, Steel, Control theory, Proportional integral controller

1. Introduction

A clear understanding of the behaviour of building structures subjected to fire is essential for the engineering community. Numerical modelling of structures has made tremendous progress in fire engineering in recent decades, and when large buildings are now designed and built, the fire situation is considered entirely by numerical modelling. This change does not mean that experimentally testing the behaviour of structural elements subjected to fire has become obsolete. Indeed, with few exceptions, a numerical model can only reproduce failure modes that have been foreseen in the model and, that have been observed experimentally. As the construction industry entails fast innovation, new structural solutions are proposed as well as new materials, such as high-performance concretes. These new solutions and new materials must undergo experimental testing before they can be modelled.

One of the main drawbacks of furnaces is that they allow for testing single elements, such as a slab, a beam, a wall, or a column. Nearly all tests completed so far have systematically been performed with fixed boundary conditions. For

*Correspondence should be addressed to: Elke Mergny, E-mail: elke.mergny@uliege.be

Published online: 10 June 2022

instance, the rotations at the ends of beams or columns are completely free or completely fixed during the duration of the test, and the same is true for the thermal elongation. However, in a real building, the boundary conditions often lay in between these extremes. Moreover, the stiffness provided by the rest of the structure at the interface with the element considered may change over time because of the structure's non-linear behaviour and, possibly, because other parts of the structure can also be subjected to the effects of the fire. Nevertheless, testing complete building structures at full scale is unrealistic not only because of time and budget constraints but also because of the limited size of the equipment available to perform fire tests.

Consequently, in the 1990s, a novel testing technique was developed in fire engineering. This technique consists of dividing the structure into a physical substructure (PS) tested in a fire test laboratory and a numerical model or numerical substructure (NS), which accounts for the remaining structure. By reducing the size of the tested element, this method overcomes the huge costs of large-scale tests while realistically reproducing the real behaviour of the element embedded in a wider structure. During the fire test, the conditions at the boundaries of the tested specimen are continuously updated to reflect the real conditions of the specimen being subjected to fire in the complete structure.

As the specimen is physically tested full-scale in a furnace while the behaviour of the rest of the structure is numerically simulated, this testing technique is generally called "hybrid testing" and is not new to structural engineering. It has been applied the past few decades, in the field of seismic engineering [1] to overcome the cost of large-scale testing. First developed in the 1970s, hybrid testing includes pseudo-dynamic testing (with and without substructuring), real-time tests, and an effective force test method. The large amount of research led to a reliable dynamic test method.

However, despite the many contributions of this research in earthquake engineering, the use of hybrid testing in fire engineering is not straightforward because of phenomena specific to temperature increase. First, the HFT must be carried out in real time because the development of thermal gradients on the section of the elements makes time scaling impossible. Second, the axial forces and stiffnesses must be considered. These forces and stiffnesses are often neglected in seismic testing, because the focus is essentially on relatively soft degrees of freedom, such as rotations and horizontal displacements (many methods in structural engineering at room temperature are indeed based on the hypothesis of axially undeformable members). Finally, applying high temperature complicates the experimental process because it is not possible to measure forces and/or displacements where and how the researchers want. In addition, the instruments must be protected. Thus, hybrid fire testing (HFT) constitutes a separate field that has its own challenges.

Research into HFT began in the 1990s. A first wave of tests were based on force control procedures, meaning that the force of the PS is updated based on the response of the numerical substructure. The first attempt was reported by Korzen et al. [2] and consisted in a one-degree-of-freedom (DOF) HFT of a steel frame with a column subjected to fire. The axial force in the specimen was adjusted as a function of the numerical substructure's elastic response to the displace-

ment of the heated column. Similarly, Robert et al. [3] attempted a multi-DOF test, but the test was stopped before failure. Later, Mostafaei [4] successfully coupled a concrete column and a multi-storey building modelled in SAFIR® [5]. Nevertheless, the axial force was controlled and adjusted every 5 min by a human operator. This approach was recently reproduced in a fully automated small-scale test reported in Pinoteau et al. [6]. These tests were pioneers in the field of HFT and have paved the way for much research. However, they were conducted for demonstration purposes. The displacements of the PS and the NS were not verified as compatible. In addition, the applied procedures were not proven to remain stable in other conditions. Further theoretical works [7] have demonstrated that force control procedures are not unconditionally stable.

Later, many displacement control procedure algorithms were developed, which means that the displacement of the PS has been updated. However, few algorithms have so far resulted in tests. Whyte et al. [8] proposed a thermo-mechanical framework for hybrid testing that extends hybrid testing of earthquake engineering to fire engineering. They conducted a one-DOF test using a small-scale element in a universal testing machine. However, the test led to stability and displacement incompatibility issues, revealing that the extension of acquired knowledge in earthquake engineering is not straightforward. Schulthess [9] presented the results of research that began in 2016, after the tests described in Whyte et al. [8]. The research aimed to develop a methodology to perform hybrid tests specific to fire engineering by solving static equilibrium equations. The stiffness of the PS at 20°C was used in the solver. The test results were compared with pure physical tests, and minor differences were observed, mainly due to the stiffness that was slightly different from one sample truss to another. Another test led in the same setup was reported in Grolimund [10] and proposed to use time scaling. However, limitations exist in both publications: the hybrid test was performed on a small-scale specimen in a well-controlled environment (universal testing machine). Usually, fire tests are performed on full-scale specimens with actuators that have limited accuracy.

Afterward, Wang et al. [11] filled this gap by testing a steel column as the PS at the Korea Institute of Construction Technology testing facilities. The numerical substructure was a multi-storey building modelled in ABAQUS®. The expected response was acceptably reproduced despite differences with numerical predictions attributed to limitations of the experimental setup. These tests allowed researchers to tackle technical issues in HFT and led to the development of a communication software to link the NS and the actuators in the furnace. Menari et al. [12] also performed a one-DOF hybrid simulation of a small-scale braced frame subjected to fire with the same communication software, demonstrating the applicability of hybrid fire simulation for fire following an earthquake event. Recently, Abbiati et al. [13] proposed an algorithm based on a finite element tearing and interconnecting (FETI) approach and a localized Lagrange multipliers method to couple the PS and NS. A dynamic relaxation algorithm was adopted to build an equivalent dynamic system that mimics the static response of substructures. This procedure was validated through a single-DOF test in Sauca et al. [14] and a multi-DOF test in Tsokanas et al. [15]. In both cases, the PS was a small-scale element

(between 46 and 91 cm) and the NS was elastic. Other conceptually different studies were developed such as Quershi [16] which proposed to modify an actuator so that it behaves like the NS. This approach is promising but still in their infancy.

The previous research has demonstrated that the HFT method is promising. However, few tests have been completed so far, and most are limited to one DOF, which reduces the application to specific structural elements, typically free in rotations at the ends, such as bars in trusses or simply supported columns. Moreover, these tests were performed considering the NS that remains at ambient temperature or, if heated, that remains in the elastic domain, which greatly simplifies the problem. The present research performed the first fully automated multi-DOF hybrid test in fire engineering with a heated NS.

The paper is divided into three sections. The first section describes the experimental setup built at Liege University to perform hybrid fire tests; the testing procedure on the algorithm developed in Mergny et al. [17]; and the case of study. Then, the results are presented and discussed. The last section concludes with a thorough discussion of the method's accuracy and impact on structural fire engineering.

2. Materials and Methods

2.1. Algorithm to Perform Hybrid Fire Testing

2.1.1. Basic Equations As developed in Sauca [18], the algorithms used to perform HFT require several conditions for successful tests. First, the interface forces of each substructure must be in equilibrium with each other, and the displacements must be compatible. If this condition is fulfilled, the correct mechanical behaviour is reproduced. Then, the system must be stable, meaning it produces a bounded output for a given bounded input. Afterward, delay must be limited. The displacements or the forces of the PS must be updated from the response of the NS, this update requires a certain amount of time, called the delay. As hybrid fire tests are real-time tests, this delay must be as small as possible. Additionally, experimental errors in instruments and actuators must be limited for accuracy. However, as delay and experimental errors are not completely avoidable, the methodology developed to perform HFT must be robust to these two issues.

For this test, a procedure based on control theory was developed. The procedure proposes a proportional integral (PI) controller designed with the initial stiffness of both substructures and consists of adjusting the interface displacements to equilibrate the interface forces of both substructures. The procedure was discussed in Mergny et al. [17] but has been adapted for testing.

Considering that d DOFs of the PS are controlled using d′ actuators, the basic equation is as follows:

$$\begin{aligned} \mathbf{u}_{C_{i+1}} &= \mathbf{u}_{C_i} + \mathbf{L}_P \mathbf{e}_{C_i^{inst}} + \mathbf{L}_J \mathbf{j}_i \\ \mathbf{j}_{i+1} &= \mathbf{j}_i + \mathbf{e}_{C_i^{inst}} \end{aligned} \tag{1}$$

$\mathbf{u}_{C_i} \in \mathbb{R}^{d' \times 1}$ is the commanded displacement sent to the electric jacks. $\mathbf{e}_{C_i^{inst}} \in \mathbb{R}^{d' \times 1}$ is the instantaneous error, and $\mathbf{j}_i \in \mathbb{R}^{d' \times 1}$ is the sum of $\mathbf{e}_{C_i^{inst}}$ over time. This error is equal to $-\left(\mathbf{f}_{C,NS_i} + \mathbf{f}_{C,PS_i}\right)$, an unbalanced force vector at the interface of the NS and PS. $\mathbf{f}_{C,PS_i}$ is the force vector that contains each force measured by the load cells, and $\mathbf{f}_{C,NS_i}$ represents the interface forces in the NS that would be obtained in virtual force cells in the NS from the internal forces$\mathbf{f}_{NS_i}$. $\mathbf{f}_{C,PS_i}, \mathbf{f}_{C,NS_i} \in \mathbb{R}^{d' \times 1}$ as there are d′ load cells for d′ actuators.

$\mathbf{L}_P \in \mathbb{R}^{d' \times d'}$ and $\mathbf{L}_J \in \mathbb{R}^{d' \times d'}$ are the gain matrices of the PI controller, which is fast acting and immediate. Moreover, if the characteristics of the system change, the integral term allows large corrections. These matrices must be designed so that successive corrections do not lead to instabilities. Additionally, the value of these gains must also be limited otherwise the system becomes oscillating.

To determine the values of $\mathbf{L}_P$ and $\mathbf{L}_J$, it is necessary to formulate the state space representation of the system. The substructures PS and NS are seen as two static subsystems described by the following static equations:

$$\mathbf{K}_{PS_i}\mathbf{u}_{PS_i} + \mathbf{f}_{PS_i}^{TH} = \mathbf{f}_{PS_i} \tag{2}$$

$$\mathbf{K}_{NS_i}\mathbf{u}_{NS_i} + \mathbf{f}_{NS_i}^{TH} = \mathbf{f}_{NS_i} \tag{3}$$

These equations are written at the interface of the substructure at a discrete time i. $\mathbf{u}_{PS_i}$ and $\mathbf{u}_{NS_i}$ are respectively the relative displacements of the PS and NS. $\mathbf{K}_{PS_i} \in \mathbb{R}^{d \times d}$ and $\mathbf{K}_{NS_i} \in \mathbb{R}^{d \times d}$ stand for the stiffness matrices, defined at the interface of the two substructures. $\mathbf{f}_{PS_i}^{TH} \in \mathbb{R}^{d \times 1}$ and $\mathbf{f}_{NS_i}^{TH} \in \mathbb{R}^{d \times 1}$ are the forces induced at the interface by thermal expansion if the displacements at the interface are fixed.

One can define $\mathbf{e}_i^{inst} \in \mathbb{R}^{d \times 1}$ as the instantaneous error between the interface forces of the PS and NS, $\mathbf{f}_{PS_i}$, and $\mathbf{f}_{NS_i}$. This error is equal to $-(\mathbf{f}_{NS_i} + \mathbf{f}_{PS_i})$ and is the unbalanced force vector at the interface of the NS and PS. In the most general case, the forces measured by the load cells are not directly equal to the internal forces. One can assume that $\mathbf{f}_{C,NS_i}$ and $\mathbf{f}_{C,PS_i}$ are linked to the internal forces of the PS and NS. $\mathbf{e}_{C_i}^{inst}$ can thus be expressed as $\mathbf{T}'\mathbf{e}_i^{inst}$, where $\mathbf{T}'$ is the transformation matrix between the interface out-of-balance forces $\mathbf{e}_i^{inst}$ and the forces measured by the load cells $\mathbf{e}_{C_i}^{inst}$.

The vector $\mathbf{e}_{C_i^{inst}}$ can be replaced by $-\mathbf{T}'(\mathbf{f}_{NS_i} + \mathbf{f}_{PS_i})$ in Eq. (1). $\mathbf{f}_{NS_i}$ and $\mathbf{f}_{PS_i}$ can then be substituted by Eqs. (2) and (3). As the displacement must be compatible, $\mathbf{u}_{NS_i} = \mathbf{u}_{PS_i}$. If one assumes that the displacement vector of the specimen $\mathbf{u}_{PS}$ is linked to one of the actuators $\mathbf{u}_C$ by a transformation matrix $\mathbf{T}''$, Eq. (1) can finally be written as follows:

$$\begin{bmatrix} \mathbf{u}_{C_{i+1}} \\ \mathbf{j}_{i+1} \end{bmatrix} = \begin{bmatrix} \mathbf{I} - \mathbf{L}_P\mathbf{T}'(\mathbf{K}_{PS_i} + \mathbf{K}_{NS_i})\mathbf{T}'' & \mathbf{L}_J \\ -\mathbf{T}'(\mathbf{K}_{PS_i} + \mathbf{K}_{NS_i})\mathbf{T}'' & \mathbf{I} \end{bmatrix} \begin{bmatrix} \mathbf{u}_{C_i} \\ \mathbf{j}_i \end{bmatrix} + \begin{bmatrix} -\mathbf{L}_P T' \left(\mathbf{f}_{NS_i}^{TH} + \mathbf{f}_{PS_i}^{TH} \right) \\ -T' \left(\mathbf{f}_{NS_i}^{TH} + \mathbf{f}_{PS_i}^{TH} \right) \end{bmatrix} \tag{4}$$

This equation is the state equation of the system. $\mathbf{u}_C$ and $\mathbf{j}$ are the state variables. $\mathbf{A}_I$ is the state matrix of the system at discrete time i:

$$\mathbf{A}_i = \begin{bmatrix} \mathbf{I} - \mathbf{L}_P\mathbf{T}'(\mathbf{K}_{PS_i} + \mathbf{K}_{NS_i})\mathbf{T}'' & \mathbf{L}_J \\ -\mathbf{T}'(\mathbf{K}_{PS_i} + \mathbf{K}_{NS_i})\mathbf{T}'' & \mathbf{I} \end{bmatrix} \tag{5}$$

2.1.2. Gain Matrices Equation (5) reveals that the state matrix $\mathbf{A}_i$ depends on the gain matrices, $\mathbf{L}_P$ and $\mathbf{L}_J$. The gain matrices must be computed in such a way that the state matrix has eigenvalues that fulfil two conditions. First, the module of these eigenvalues must be lower than 1 during the entire test to ensure process stability. Then, the gain matrices must ensure controller reactivity. If the value of the gain increases, the corrections also increase, and the controller is thus more reactive.

$\mathbf{L}_P$ and $\mathbf{L}_J$ are considered diagonal. Therefore, one commanded displacement $\mathbf{u}_C$ is updated with the error of the related interface force $\mathbf{f}_C$. Corrections are made as if the DOFs were decoupled. This approximation greatly simplifies the design of the gain matrices. To determine the d′ diagonal terms of $\mathbf{L}_P$ and $\mathbf{L}_J$, the following equation is solved:

$$|\mathbf{I}z - \mathbf{A}_0| = (z - \lambda_1)(z - \lambda_2)\dots(z - \lambda_{2d'}) \tag{6}$$

The first member is the characteristic polynomial of the state matrix $\mathbf{A}_0$, which depends on the gain values that are the unknowns. The state matrix is noted as $\mathbf{A}_0$ because the initial values of stiffness of the substructures are used, meaning the stiffness at room temperature (or at i = 0, before heating). The stiffness of the NS can be computed, and the stiffness of the PS is not necessarily known but can be estimated. As the roots of $|\mathbf{I}z - \mathbf{A}_0|$ are the eigenvalues of $\mathbf{A}_0$, the second member is a polynomial with the roots equal to the eigenvalues necessary for the process and calculated beforehand. There is no single method for computing these eigenvalues. The one chosen for this test is detailed in Sect. 2.4.

2.1.3. Procedure The final block diagram of the procedure is displayed in Figure 1. At each time step, the displacement $\mathbf{u}_{C_i}$ is updated based on the error $\mathbf{e}_{C_i^{inst}}$, as well as the sum of this error over time. Then, the relative displacements of the PS are measured, and the corresponding displacements of the NS are computed, possibly using corotational transformations. This point is detailed in Sect. 2.3.

The compatibility of displacement is ensured by the procedure because the same displacements are applied to the substructures. The equilibrium of forces and the stability depend on the gain matrices. The delay depends on the size of the time

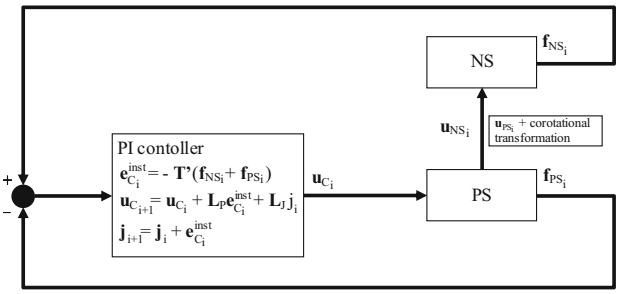

Figure 1. Block diagram.

step between two updates, which may be an issue for force equilibrium. If the delay increases, the time step between two updates increases and the system takes more time to restore equilibrium. As the temperature is continuously increasing during the test, the time step between two updates must be small enough to follow changes in interface forces due to temperature increases in the material. Concerning the experimental errors, measurement errors and control errors [19] can lead to incompatibility between the NS and PS displacements, and therefore, these errors should be limited as much as possible [19].

2.2. Reference Structure and Substructuring

The reference structure was a two-storey half-scaled building with four longitudinal bays, as illustrated in Figure 2a. This structure was composed of 1.3 m steel beams (HS160 × 80 × 5) and 1.3 m columns (HS80 × 5). The PS was a HS80 × 5 steel column located at the edge of the building in a heated compartment. The remaining structure, the NS, was modelled in the software SAFIR. The PS was heated at a rate of 6°C/min, which is consistent with the heating of a protected steel member. The rest of the compartment was heated at a rate of 5°C/min.

After substructuring, six DOF $\mathbf{u}_g$ at the interface were global, as depicted in Figure 2b. Since the PS was a floating structure, controlling the six DOF with six actuators was practically inconvenient. Three rigid body modes were fixed by the specimen's supports, which left three DOFs to be controlled. The specimen was tested with a roller support and a pinned support. The interface displacements of the PS are the elongation of the column and two rotations at the ends of the element. The three displacements measured with the displacement transducers and the inclinometers are the relative displacements.

The link between the six global DOFs $\mathbf{u}_g$ and the relative displacement $\mathbf{u}_{PS}$ is given by the corotational theory (see Figure 3) and is found in Urthale and Reddy [20]:

$$\begin{aligned} \mathbf{u}_{PS}[1] &= L - 1.3 = u \\ \mathbf{u}_{PS}[2] &= \mathbf{u}_g[3] - \alpha \\ \mathbf{u}_{PS}[3] &= \mathbf{u}_g[6] - \alpha \\ L = \sqrt{\left(\mathbf{u}_g[1] - \mathbf{u}_g[4]\right)^2 + \left(1.3 + \mathbf{u}_g[5] - \mathbf{u}_g[2]\right)^2} &= 1.3 + u \\ \alpha = \ \text{atan}\left(\frac{\mathbf{u}_g[4] - \mathbf{u}_g[1]}{1.3 + \mathbf{u}_g[2] - \mathbf{u}_g[5]}\right) & \end{aligned} \tag{7}$$

α is the rigid body rotation and L is the length of the column. Regarding the NS, these relative displacements (local DOFs) must be transformed into global DOF. The displacements that must be applied to the NS in SAFIR are the following:

- The movements of translations resulting in the elongation u of the column condensed by imposing the relative distance $1.3 + u$ between the two extremities of the column
- Two rotations to which rigid body rotations are added

The transformations are as follows:

$$\mathbf{u}_{NS}[1] = u \quad \mathbf{u}_{NS}[2] = \mathbf{u}_{PS}[2] + \alpha \quad \mathbf{u}_{NS}[3] = \mathbf{u}_{PS}[3] + \alpha \tag{8}$$

The relative distance between two nodes was imposed using the method of Lagrange multipliers, which allows one to find the local maxima and minima of a function subjected to equality constraints. This method was implemented in SAFIR for HFT. The rigid body rotation α results from the four global translation components of $\mathbf{u}_g$ and is thus not directly available. The rigid body rotation of the previous time step was chosen.

Figure 2c presents the displacements applied to the PS and NS. The rotation of rigid body of the NS is negative unlike in Figure 3, which provides the general case

2.3. Experimental Setup

2.3.1. Test Setup and Specimen An experimental setup was built in the Fire Test Laboratory of Liege University to perform hybrid fire tests. The setup consists of two parallel steel frames (Frame 1 and Frame 2 in Figure 4) bolted on two horizontal beams and braced by diagonal elements. Three electric jacks were mounted on supports and applied displacements through cross struts where hinges were bolted. These actuators were 100 kN-capacity trapezoidal screw jacks: the rotation of the worm is transformed into axial translation of the screw using the rotation of the motor. This setup enables testing steel columns from 1.3 to 1.5 m long. Compared to hybrid tests made on small material samples, the dimensions of the specimen are large enough to involve all difficulties linked to real size tests; however, using half scale specimens provides the requested flexibility that allows for testing various solutions at a reasonable cost in different attempts in the context of a research project.

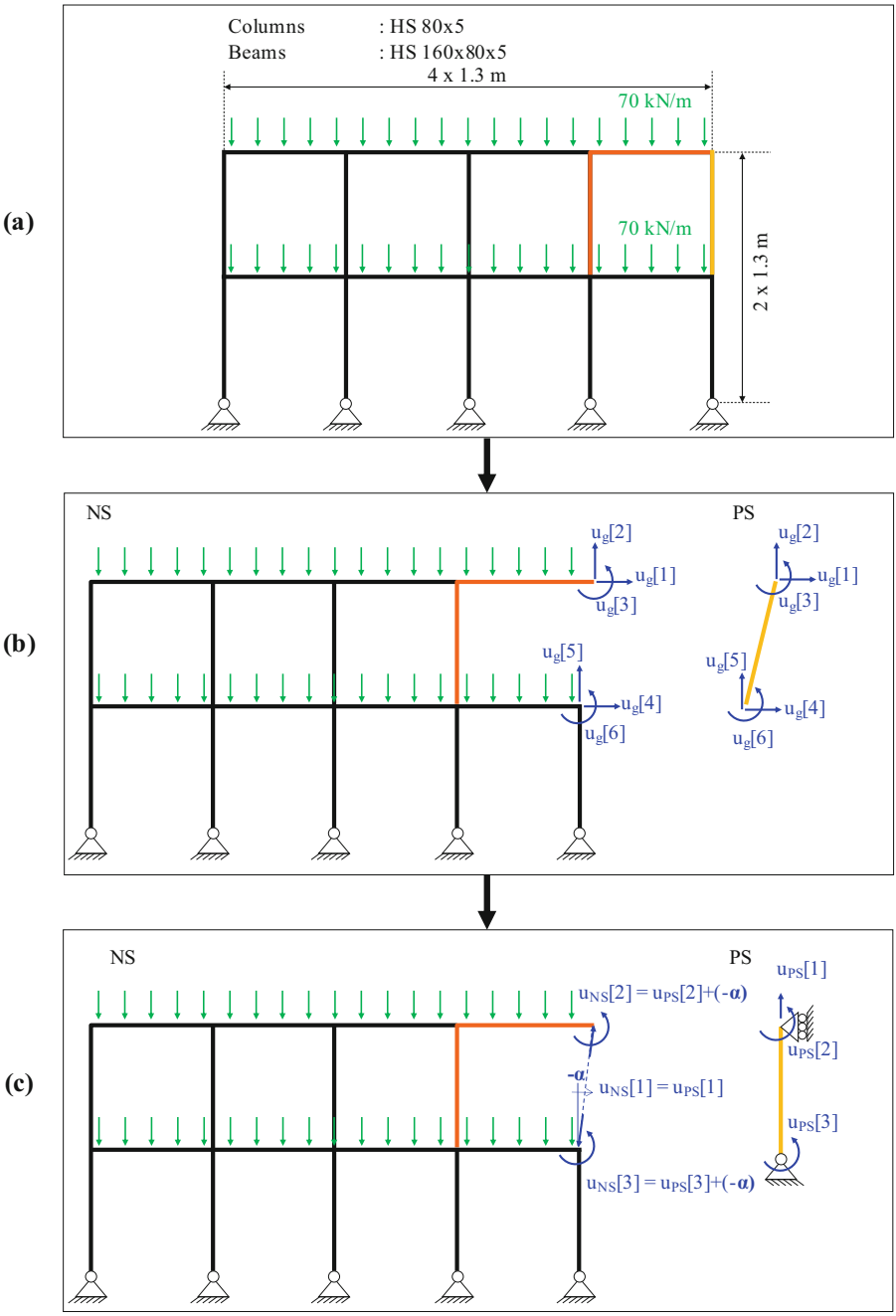

Figure 2. Three-DOF test: the NS and PS (a) reference structure, (b) after substructuring, (c) after substructuring and corotational transformation.

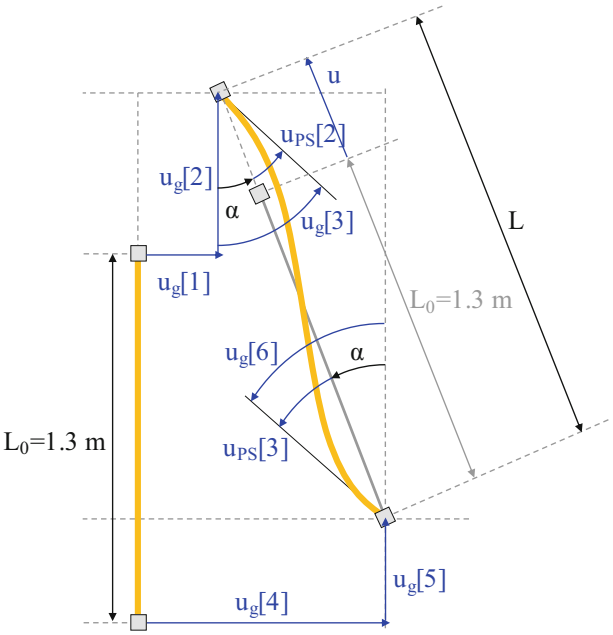

Figure 3. Corotational transformations.

Flexible ceramic pad heaters were used for heating the specimen, which, compared to a gas furnace, results in easier integration of displacement transducers, inclinometers, and load cells in the setup. There were four pads on the column. The feedback variable of each pad heater is the temperature of a thermocouple welded on the specimen, on the middle of the area covered by one pad. The column was wrapped with ceramic fibre mats to limit heat losses to the environment.

Up to three DOFs of a column can be controlled in this setup. Three tests were performed during this research: a one-DOF test, a two-DOF test, and a three-DOF test. The present paper focuses on the three-DOF test. The setup is displayed in Figure 5. Details about the other tests are found in Mergny [21].

The tested specimen is depicted in Figure 6. The two extremities of the PS were welded to two HEB100 beams serving as lever arms. Two steel plates were welded to these beams, in line with the columns to receive the hinges. The column was tested upside down as illustrated in Figure 5, compared to Figure 2c.

The elongation was measured with four potentiometric displacement transducers. Since the loading frame had some flexibility, the elongation of the column could not be determined by simply measuring the displacement of the moving cross struts. The transducers were thus not fixed directly on the loading frame; on each side of the column, two sensors (one at each end of the column) were fixed to an OSB plank, which was itself fastened at a single point (in its middle) to the profile of the loading frame. The elongation of the loading frame was thus eliminated as was any eventual displacement of the point at which the OSB plank was fastened. Although thermal elongation of timber-based products such as OSB is

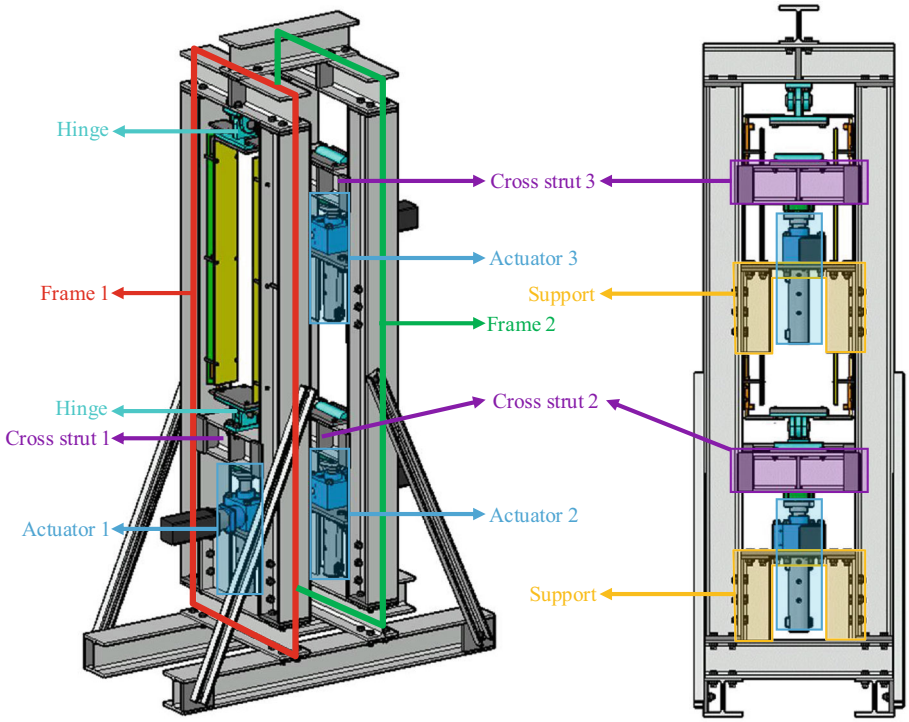

Figure 4. Experimental setup.

low, gypsum plates were nevertheless fastened between the OSB planks and the insulating map that wrapped the specimen. The detail is provided in Figure 7. The rotations were measured with single axis inclinometers. Two inclinometers lay on the lever arm to measure the rotation (“Inclinometer 1” and “Inclinometer 2” in Figure 5).

The load cells (“Load cell 1”, “Load cell 2”, “Load cell 3” in Figure 5) were between the cross struts and the actuators (“Actuator 1”, “Actuators 2”, and “Actuators 3” in Figure 5). The combinations of the measured forces allow one to compute the internal forces. Notably, the load cells work only in compression. This limitation is not a problem for the axial force because the column was expected to remain in compression during the whole test. However, unlike the normal force, the moment could change the sign toward the end of the test. As the setup does not allow the actuators to pull on the load cells, the cross strut was preloaded by steel masses to apply a bending moment of − 1700 kNm. The cross struts were attached to the lever arm with four threaded rods bolted to a steel plate. A cylinder was placed between the plate and the lever arm.

The column was heated with four electrical pad heaters controlled with a thermocouple located in the middle of each heated zone. The temperatures of the NS sections were pre-calculated with SAFIR.

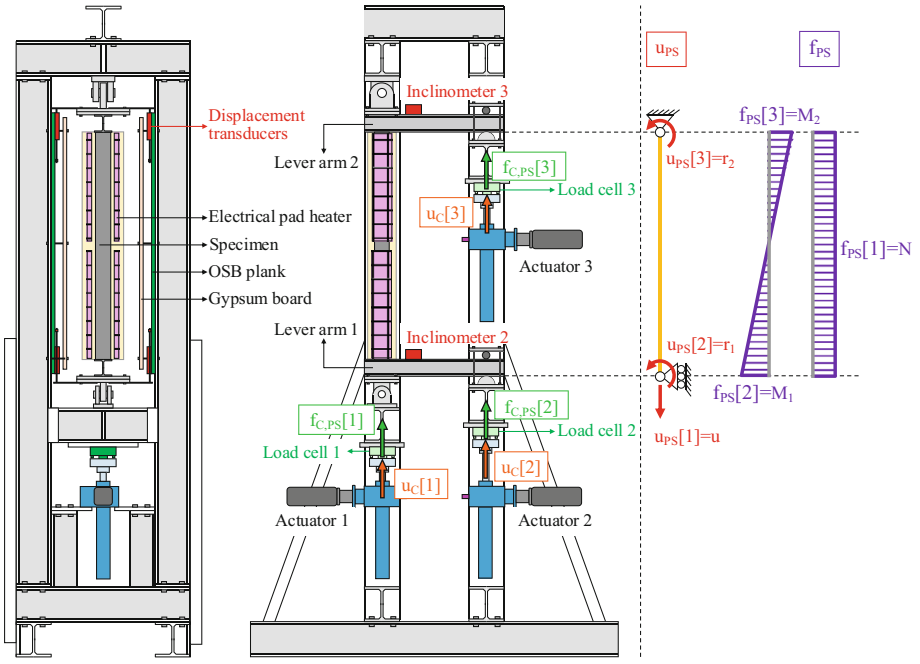

Figure 5. Testing configuration.

Figure 6. Specimen.

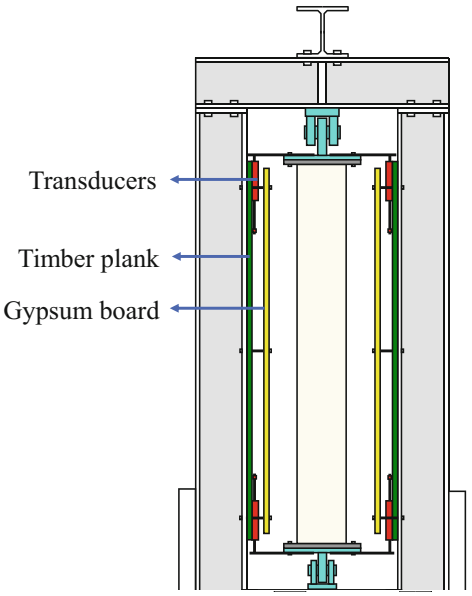

Figure 7. Details of the transducers.

2.3.2. Testing Procedure The testing procedure presented in Sect. 2.1.3 is illustrated in Figure 8 and was performed as follows:

1. At the beginning of the time step, forces and displacements of the PS were measured by the laboratory datalogger and sent to the computer.

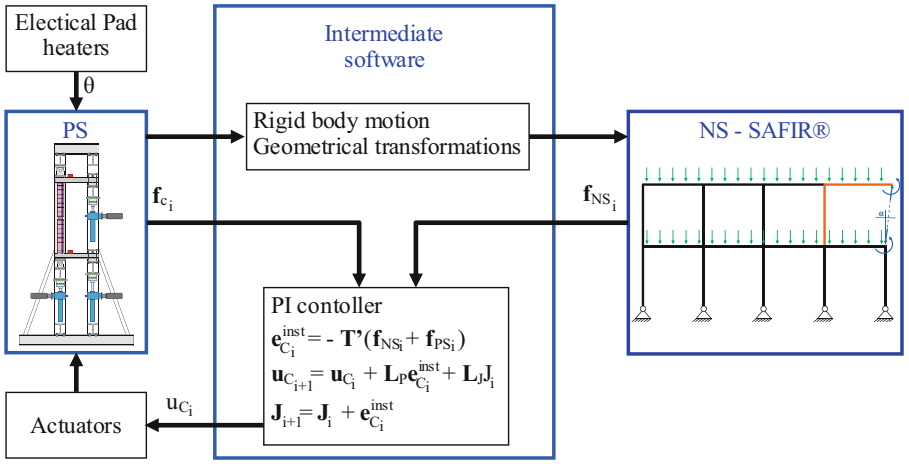

Figure 8. Testing architecture.

2. The measured displacements were imposed to the NS (considering geometrical transformations and rigid body motion). The NS was a non-linear finite element model in SAFIR. The interface forces were computed.
3. The forces of the PS and NS were sent to intermediate software that ensured the connections between the two substructures. This software deals with the PI control and corotational transformations. The instantaneous error was calculated. The new commanded displacement $\mathbf{u}_C$ and the integral term $\mathbf{j}$ were then computed with Eq. (1).
4. The new command $\mathbf{u}_{C_{i+1}}$ was sent to the actuator and applied linearly to the PS until the end of the time step.

The heating of the two substructures did not start immediately. The load of the NS was first applied linearly at 20°C in 20 min, after which the load was maintained for 5 min at room temperature before heating was applied.

During the time step, the actuators did not stop moving. At a time $t_i + \Delta t$, if $\mathbf{u}_{C_{i+1}}$ was computed before the end of the time step, each displacement was interpolated between $\mathbf{u}_{C_i}$ and $\mathbf{u}_{C_{i+1}}$; otherwise, it was extrapolated:

$$\text{Interpolation} \quad \mathbf{u}_{C_{i+1}} \text{ is computed} \quad \mathbf{u}_{C_{t_i+\Delta t}} = \frac{\mathbf{u}_{C_{i+1}} - \mathbf{u}_{C_i}}{T}\Delta t \tag{9}$$

$$\text{Extrapolation} \quad \underset{\text{has not yet been computed}}{\mathbf{u}_{C_{i+1}}} \quad \underset{\substack{\text{a,b obtained by linear regression on the position at} \\ \text{the four previous time steps}}}{\mathbf{u}_{C_{t_i+\Delta t}} = a(t_i + \Delta t) + b} \tag{10}$$

T is the time step between two updates. No iteration was performed within each time step because, as temperature in the furnace changes continuously, achieving a converged solution through iterations in each time step would be challenging.

2.4. Design of the Gain Matrices

As linear control is used, the gain matrices were constant during the test and were determined with the mechanical proprieties of the substructures at room temperature. The consequences of this strategy are discussed in this section and in the results in Sect. 3.2.

The initial values of the interface stiffness of the NS and the PS were thus first determined. The stiffness matrix of the NS $\mathbf{K}_{NS_0}$ was computed using the method proposed by Sauca [18, pp. 146–148]. The method consists of applying a unit displacement to the NS at the interface and calculating the resulting three reaction forces. The stiffness matrix of the PS $\mathbf{K}_{PS_0}^{EST}$ was estimated with the analytical formulation of the stiffness matrix (considering E = 210 GPa). All the values presented below are expressed in [N], [m], and [rad]:

$$\mathbf{K}_{\mathrm{PS}_0}^{\mathrm{EST}} = \begin{bmatrix} \frac{EA}{L} & 0 & 0 \\ 0 & \frac{4EI}{L} & \frac{2EI}{L} \\ 0 & \frac{2EI}{L} & \frac{4EI}{L} \end{bmatrix} = 10^3 \begin{bmatrix} 237461 & 0 & 0 \\ 0 & 885 & 442.5 \\ 0 & 442.5 & 885 \end{bmatrix}$$
$$\mathbf{K}_{\mathrm{NS}_0} = 10^3 \begin{bmatrix} 4944 & 170 & -3895 \\ 170 & 4040 & -130 \\ -3895 & -130 & 4827 \end{bmatrix} \tag{11}$$

The state matrix of the system (4) is a sixth order system and has six eigenvalues. The eigenvalues of the state matrix presented in Eq. (5) must then be adjusted by computing the gain matrices. These eigenvalues must be adjusted to stabilise the system and allow controller reactivity. Stability was obtained by imposing a module lower than one. The reactivity is related to the time proprieties. Unlike first order or second order systems, for sixth order systems, the link between the eigenvalues and the time proprieties (and thus reactivity) are not well known in the literature.

To circumvent this problem, the controller was designed to obtain a pair of two dominant eigenvalues with the other equal to 0. This design enables the approximation of a sixth order system by a second order system that can be linked to the time parameters of the step response. The module of the pair of dominant eigenvalues must be lower than one, and their module is chosen to adjust controller reactivity. The dominant eigenvalues λ were computed with a well-known equation of control theory:

$$\lambda = \exp\left(-2.72\frac{T}{T_r}\right) \tag{12}$$

The value λ depends on T, which is the sample time, or the time step between two updates, and the rise time T_r defined as the transition time from 10 to 90% of a target value. Regarding the time taken by SAFIR to calculate the NS, the time step possible between two updates is 3 s. Thus, T = 3 s. This time specifies how often the controller samples the measured process variable and computes and transmits a new controller output. If this time step increases, the corrections are less efficient as the controller acts less often.

The rise time was determined by a succession of cold loading for several rise times (and therefore different pairs of eigenvalues). Some cases are displayed in Figure 9. The case with a rise time of 12 s resulted in a reactive controller without excessive oscillations.

The double eigenvalue λ was thus computed with Eq. (13):

$$\lambda = \exp\left(-2.72\frac{3}{12}\right) = 0.51 \tag{13}$$

The 3×3 transformation matrices $\mathbf{T}'$ and $\mathbf{T}''$ were then computed. The normal force $f_{PS}[1] = N$ is the sum of the two forces measured with "Load cell 1" and

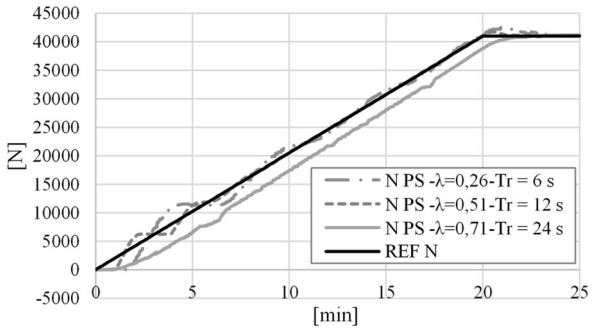

Figure 9. Cold test to determine the rise time.

"Load cell 2". The bending moment $f_{PS}[2] = M_1$ consists of two terms. First is the force of "Load cell 2" multiplied by the lever arm a_1 equal to 0.61 m. Then, due to assembly inaccuracies in the set-up, the first actuator was slightly offset by 2.5 mm toward the inside. As a result, a contribution from the force of "Load cell 1" had to be considered. The bending moment $f_{PS}[2] = M_2$ is equal to the force measured with "Load cell 3" multiplied by a_1. The following matrix $\mathbf{T}'$ gives the relationship between the interface forces and the forces measured by the load cells, as illustrated in Figure 10a:

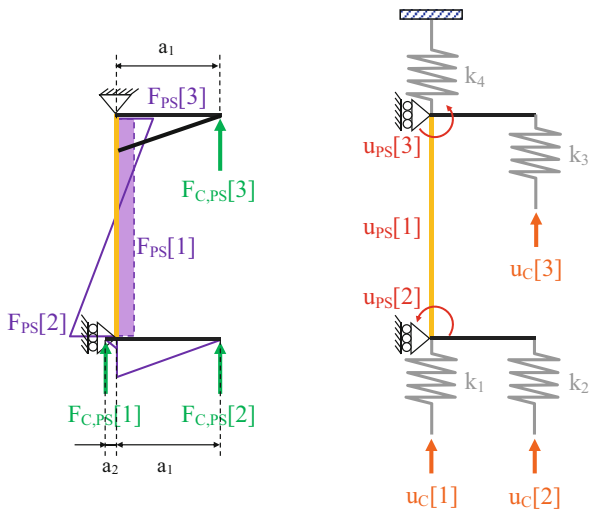

(a) *Model to determine T'* **(b)** *Model to determine T''*

Figure 10. Transformation matrices.

$$\mathbf{T}' = \begin{bmatrix} 1 & 1 & 0 \\ a_1 & a_2 & 0 \\ 0 & 0 & a_1 \end{bmatrix}^{-1} \tag{14}$$

The relationship between $\mathbf{u}_{PS}$ and $\mathbf{u}_C$ is more complex because it depends on the stiffness of the frame and of the HEB100 lever arms. A simplified plane frame model of the specimen in the setup is illustrated in Figure 10b. The springs represent the stiffness of the setup. The parameters k_1, k_2, and k_3 are associated with the actuator supports, and k_4 corresponds mainly to the stiffness of the frame where the specimen is bolted (Frame 1 in Figure 4). The stiffnesses k_1, k_2, k_3, and k_4 were calibrated with measurements on the setup and a numerical model of the setup. The matrix $\mathbf{T}''$ consists of large expressions presented in Mergny [21, Appendix D].

Finally, the gain matrices were computed by solving the following equation:

$$|\mathbf{I}z - \mathbf{A}_0| = (z - 0.5134)^2 z^4 \tag{15}$$

Using a MATLAB® procedure, the following gain matrices were obtained:

$$\mathbf{L}_P = 10^{-9} \begin{bmatrix} 4.502 & 0 & 0 \\ 0 & 65.366 & 0 \\ 0 & 0 & 123.58 \end{bmatrix} \quad \mathbf{L}_J = 10^{-9} \begin{bmatrix} 0.186 & 0 & 0 \\ 0 & 15.352 & 0 \\ 0 & 0 & 57.778 \end{bmatrix} \tag{16}$$

However, two questions remain:

- As the gain matrices $\mathbf{L}_P$ and $\mathbf{L}_J$ are constant, is the stability of the system ensured during the entire test? In fact, the gain matrices are determined with initial stiffness matrices that ensure the eigenvalues are lower than 1 at room temperature, but is the stability ensured during the test when the stiffness of the substructures degrades because of fire?
- Since the initial stiffness of the PS can only be estimated, what are the effects of overestimating or underestimating the stiffness on the stability of the system?

For a one-DOF system, if the gains matrices lead to a stable system at room temperature, the system remains stable during heating [21]. The system also remains stable if the gain matrices are designed with an estimation $\mathbf{K}_{PS_0}^{EST}$ larger than $\mathbf{K}_{PS_0}$. Instabilities can appear if the initial stiffness is underestimated.

For multi-DOF systems, the equations are much more complicated, and finding rules similar to those for a one-DOF system is difficult. Two methods can be used to verify the stability in this case:

- The estimation of the eigenvalues during the test with simplified equations
- The numerical simulation of the hybrid test.

The stability of the process is hereunder verified with the two processes.

2.4.1. Simplified Equations This method consists of explicitly computing the eigenvalues of the state matrix $\mathbf{A}_i$ where an approximation of the degradation of $\mathbf{K}_{PS_0}$ is considered. During the test, $\mathbf{K}_{PS_i}$ decreases as $\epsilon\mathbf{K}_{PS_0}$ with real $\epsilon \in [0;1]$. The stiffness of the NS $\mathbf{K}_{NS}$ is not degraded. The simplified state matrix $\mathbf{A}(\epsilon)$ is thus as follows:

$$\mathbf{A}(\in) = \begin{bmatrix} \mathbf{I} - \mathbf{L}_P\mathbf{T}'(\in \mathbf{K}_{PS_0} + \mathbf{K}_{NS_0})\mathbf{T}'' & \mathbf{L}_J \\ -\mathbf{T}'(\in \mathbf{K}_{PS_0} + \mathbf{K}_{NS_0})\mathbf{T}'' & \mathbf{I} \end{bmatrix} \tag{17}$$

To verify the stability, the eigenvalues of $\mathbf{A}(\epsilon)$ are explicitly computed for $\epsilon \in [0,1]$. The resulting poles are displayed in Figure 11, which reveals that they lie in the unit circle. The system is thus stable.

2.4.2. Virtual Hybrid Test Virtual hybrid fire testing consists of virtually simulating the hybrid test by replacing the PS and the actuators with a numerical simulation that approximates the behaviour of the specimen and the setup. A specific tool was developed within this research to conduct virtual tests. This tool performed a hybrid test with two substructures modelled in SAFIR. The numerical simulation of the PS corresponds to the simplified model depicted in Figure 10b that accounts for the stiffness of the setup.

A time step of 3 s was considered. Experimental errors in displacements and forces of the PS were also introduced, using Sect. 4.3.5 of the "Guide to the expression of uncertainty in measurement" [22]. The available information indicated the probability that the value of the input quantity lies within an interval $[a^-, a^+]$ and is equal to 0.5. In this case, one can assume a normal distribution of

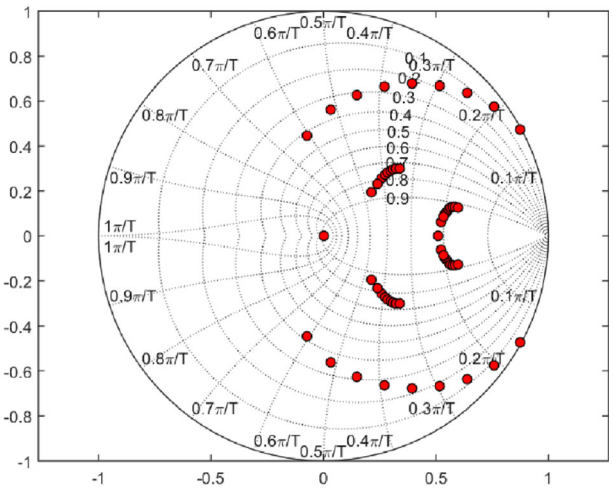

Figure 11. Three-DOF test: Predicted location of the poles.

values of displacements or forces with standard deviation σ equal to 1.48 s, "s" standing for the half-width of the interval, $\frac{a^+ - a^-}{2}$. The following intervals were assumed for the instruments:

- ± 0.1% of the full scale for the load cells
- ± 0.02% of the full scale for the inclinometers
- ± 0.02 mm for the displacement transducers.

The highest capacity of the load cell is equal to 100 kN and the range of the inclinometer is ±14°.

The results of the virtual test are displayed in Figure 12, which illustrates the evolution of the displacements and the forces. The results are compared with the simulation of the complete structure (the "REF" curves). As expected by the simplified equations, the system is stable. The method also reproduces the complete behaviour of the structure despite delay and experimental error. This conclusion is only valid for this test and cannot be generalized to all HFTs.

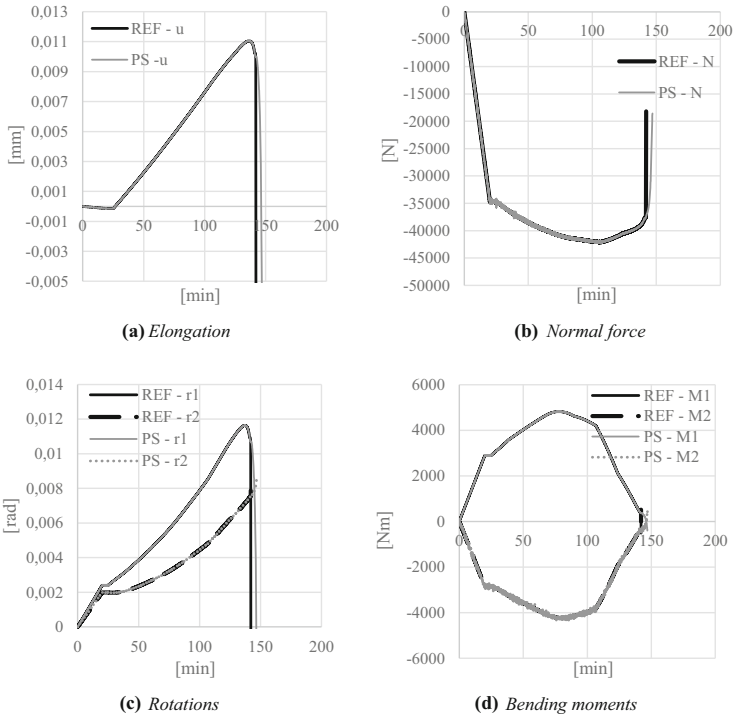

(a) *Elongation* **(b)** *Normal force*

(c) *Rotations* **(d)** *Bending moments*

Figure 12. Virtual hybrid fire testing.

3. Results and Discussion

3.1. Test Results

The test was performed on 8 October 2020. Figure 13a–c display the column during the test and after buckling.

Figure 14 presents the force–displacement relationship. Forces and displacements as a function of time are given in Figure 17a–f. Rotations, axial displacement, and forces increased linearly during the loading phase. Then, the load was maintained. The column was shortened by 0.211 mm, and the normal force stabilised around − 34.8 kN. After 25 min, the heating started, and the NS restrained the thermal expansion of the PS. Thus, the normal force increased linearly. When the steel temperature reached 200°C in the PS (just before 60 min), the Young modulus degradation began, and as Figure 14a reveals, the curve gradually flattens out. The force–displacement relationship is almost constant around 400°C and, at a temperature of around 550°C, the displacement and force started to decrease due to plastic deformation of the specimen. Buckling occurred at 624°C. The specimen buckled partially out-of-plane. As expected, the system was stable during the entire test.

The shape of these curves is different from what one might apply to the element during a traditional test in which the forces M and N remain constant.

3.2. Interface Error

The substructuring approach can only yield accurate results if displacement compatibility and force equilibrium are satisfied at the interface between the NS and the PS. The compatibility of the displacements is ensured by the testing process, as the displacements of the specimen are directly applied to the NS. The equilibrium between forces is a crucial point as it quantifies and assesses the quality of the algorithm.

(a) *During the test (front)* **(b)** *During the test (behind)* **(c)** *After buckling*

Figure 13. Three-DOF test.

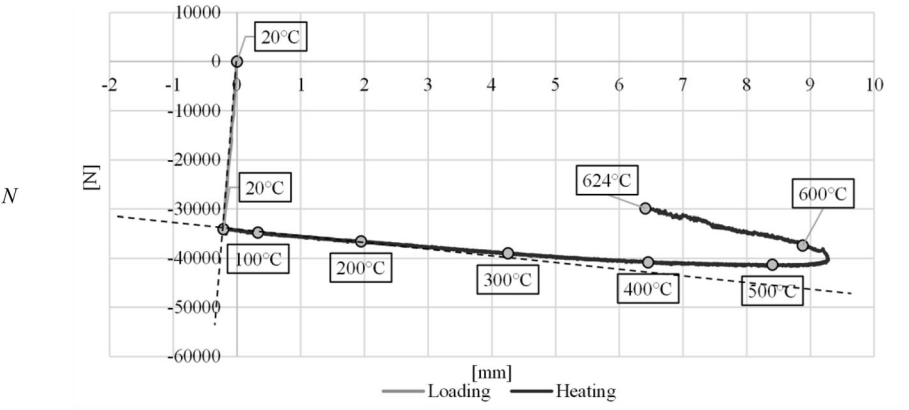

(a) *Elongation-Normal force*

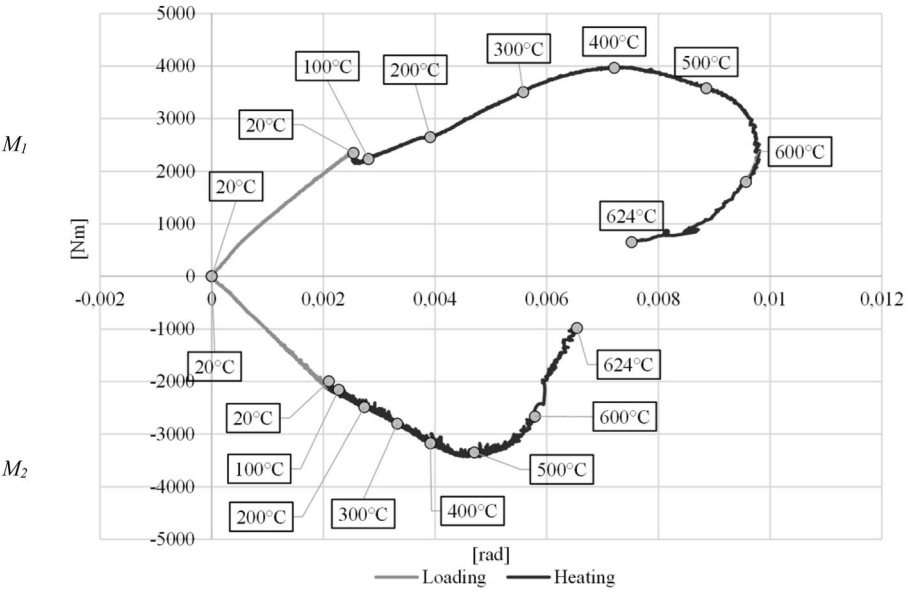

(b) *Rotation-Bending moment*

Figure 14. Three-DOF test: force–displacement relationship.

Figure 15a depicts the interface normal force between the NS (“N NS”) and PS (“N PS”) as a function of time. The normal forces at the interface between the NS and PS are in equilibrium, with a slight gap at the end. The relative error Err N displayed in Figure 15b is computed as follows:

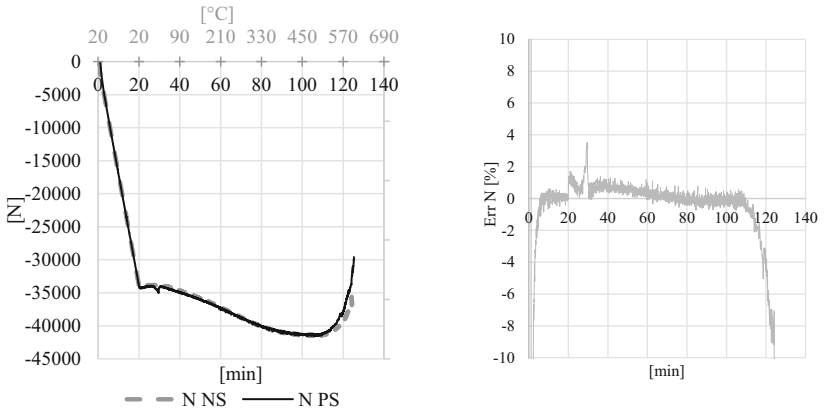

(a) *Normal force at the interface of the NS and PS* **(b)** *Relative instantaneous error Err N*

Figure 15. Three-DOF test: equilibrium of the normal force.

$$\text{Err N} = \frac{f_{NS}[1] + f_{PS}[1]}{f_{PS}[1]}[\%] = \frac{f_{NS}[1] + f_{C,PS}[1] + f_{C,PS}[2]}{f_{C,PS}[1] + f_{C,PS}[2]}[\%] \tag{18}$$

$f_{C,PS}[1]$ and $f_{C,PS}[2]$ are the forces measured by "Load cell 1" and "Load cell 2".

The relative error is high at the start of the test (more than 100%[1] because $f_{PS}[1] \approx 0$ and $f_{NS}[1] \neq 0$ at the first time step) but rapidly decreases to approach perfect equilibrium. The value is then under 2% during the loading. The error increases again when the heating begins. This increase is explained by the fact that, while maintaining the load on the column ($t \in [20\text{ min}, 25\text{ min}]$), the instantaneous error and the integral term are decreasing because the interface forces are increasingly equilibrated. When the heating starts, the instantaneous error increases, and the displacement is corrected. However, the correction is not sufficient at the beginning as the integral term needs some time steps to increase again and to generate a reactive behaviour of the proportional integral controller. Consequently, the normal force increases too fast at the early beginning of the heating. The situation is, however, quickly stabilised by the algorithm. During the test, the value of the error remained below 2% until failure when an increase of the interface error was observed. When the column collapsed, high non-linearities and a dynamic behaviour led to the corrections not being sufficiently reactive to reach equilibrium.

The interface bending moments M_1 and M_2 and relative errors Err M_1 and Err M_2, computed by Eqs. (19) and (20), are provided in Figure 16.

$$\text{Err } M_1 = \frac{f_{NS}[2] + f_{PS}[2]}{f_{PS}[2]}[\%] = \frac{f_{NS}[1] + a_1 f_{C,PS}[1] + a_2 f_{C,PS}[2]}{a_1 f_{C,PS}[1] + a_2 f_{C,PS}[2]}[\%] \tag{19}$$

[1] The limits of the vertical axes of the graph in Figure 14 have been reduced for better understanding.

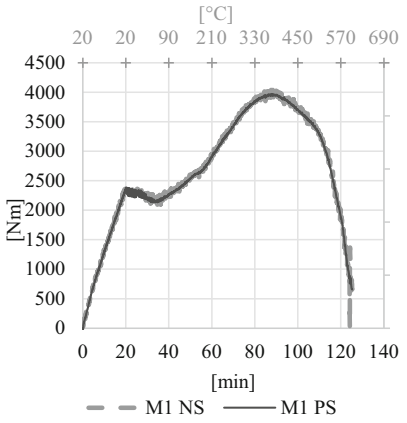

(a) Bending moment at the interface of the NS and PS M_1

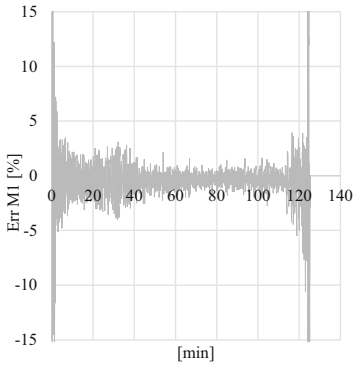

(b) Relative instantaneous error Err M_1

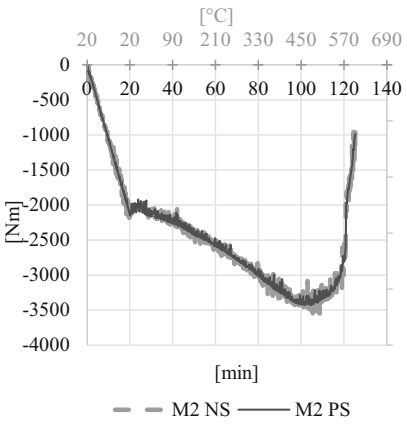

(a) Bending moment at the interface of the NS and PS M_2

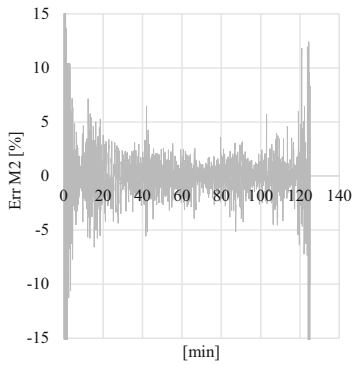

(b) Relative instantaneous error Err M_2

Figure 16. Three-DOF test: equilibrium of the bending moments.

$$\text{Err } M_2 = \frac{f_{NS}[2] + f_{PS}[2]}{f_{PS}[2]}[\%] = \frac{f_{NS}[1] + bf_{C,PS}[3]}{bf_{C,PS}[3]}[\%] \tag{20}$$

$f_{C,PS}[3]$ is the force measured by "Load cell 3". The interface errors varied during the test but usually remained in the interval $[-5\%, +5\%]$.

Figure 16a illustrates the curve of bending moment M_1 of the NS is not smooth and has numerous spikes. These variations are explained by the inclinometer measurement being directly used to calculate the rotation applied to the NS. This rotation presents small variations caused by the noise of the inclinometer, which is in the order of 10^{-5} rad. Equation (11) explains that the order of magnitude of

the diagonal term of $\mathbf{K}_{NS_0}$ is 4×10^6. Therefore, variations of 40 Nm are expected in the bending moment of the NS, which corresponds to the peaks present in the graph.

These spikes are higher in the graph of M_2, and both the NS and PS present these variations. This difference between the two moments was slightly visible on the graph of the virtual test (Figure 12d) and is explained as follows:

– The rotational stiffness of the NS is higher at the bottom (see stiffness matrix in Eq. (11)), so the experimental errors increase the spikes;
– The gains $\mathbf{L}_P$ and $\mathbf{L}_J$ related to this DOF are higher, especially the $\mathbf{L}_J$ term. In this three-DOF test, the hypothesis of decoupled DOFs (discussed in Sect. 2.4) is questionable, resulting in gains that entail less satisfying behaviour and overshoots.

3.3. Comparison with Numerical Simulation

The test was simulated with the steel temperatures recorded in the steel column introduced in the PS model. The column was modelled with a 3D beam finite element and an initial out-of-plane geometrical imperfection of 2.6 mm to allow an eventual development of out-of-plane buckling, as observed during the test.

Results of the axial displacement and the rotations computed in the PS as a function of time are depicted in Figure 17a, c, and e, whereas corresponding normal force and bending moments of the specimen are presented in Figure 17b, d, and f.

The normal force and the axial displacements of the numerical simulation are close to those measured in the test. The errors are small during most of the test and are less than 1 mm for the displacement and 1 N for the force, except at the end of the test for the reasons explained in Sect. 3.2. The rotations and the bending moments follow similar trends, but there are differences, especially in the rotations. A possible cause is the location of the inclinometers, which are not exactly at the base of the column but at a distance of 120 mm because the inclinometer had to be protected from the heat. Furthermore, the numerical model of the column is based on the steel constitutive model of EN 1993-1-2, and there may be some differences in the behaviour of steel in the test. Figure 18 illustrates the force–displacement relationship at the interface of the column and the rest of the structure, with similar trends in the simulation and in the test. These comparisons suggest that the hybrid test allowed for an accurate representation of that column's behaviour if subjected to fire in a complete structure.

4. Conclusion

Hybrid testing is an appealing method in structural engineering as it combines the benefits of both numerical simulations and experimental testing. However, the review of the state of the art also reveals that few experimental hybrid tests have been performed, and most had severe limitations: small specimen size, linear

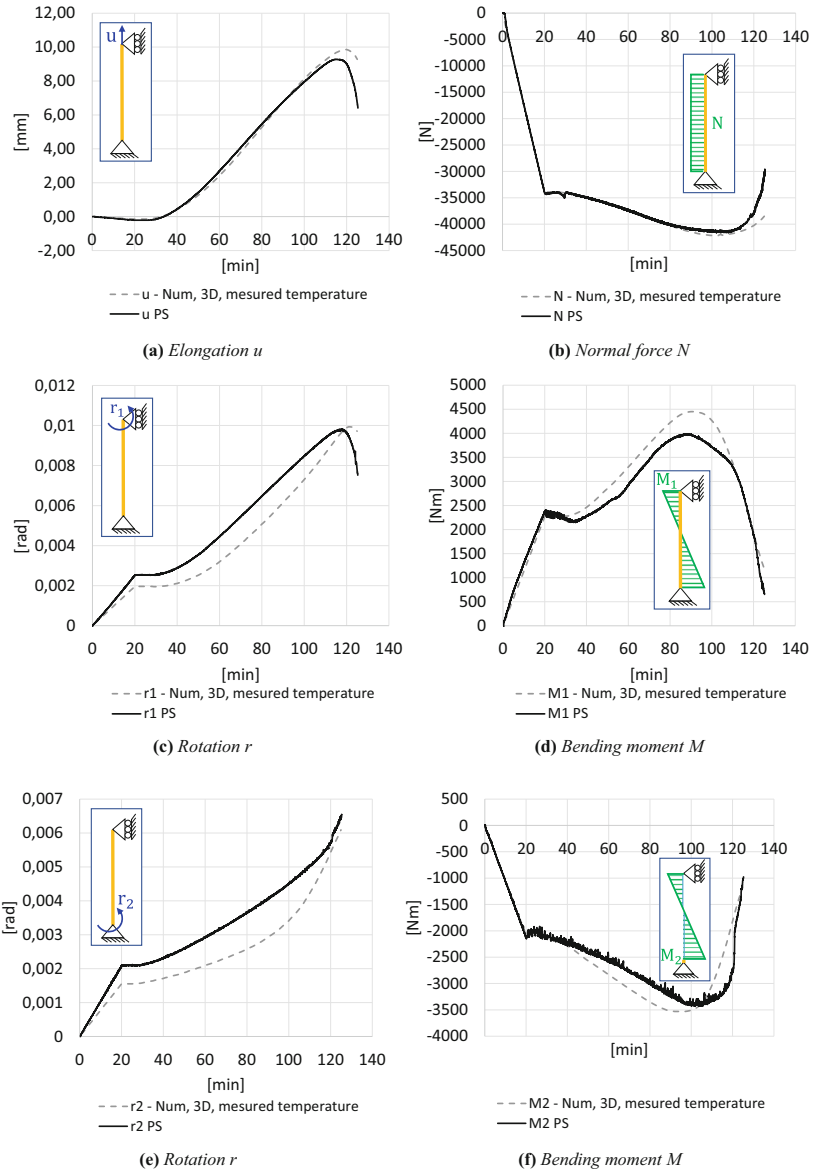

Figure 17. Three-DOF test: comparison with numerical simulations.

response of the numerical structure, lack of convergence, manual procedure, one single DOF.

The experimental test performed in this research significantly advances HFT. For the first time, a fully automated multi-DOF test was performed on a half scale specimen considering a non-linear response of the numerical structure that

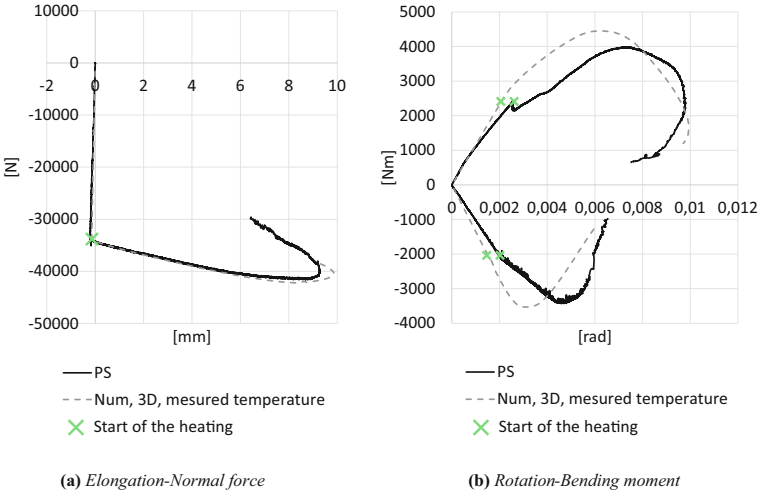

(a) *Elongation-Normal force* **(b)** *Rotation-Bending moment*

Figure 18. Three-DOF test: force–displacement relationship.

was itself partially heated. Stability, compatibility of displacement, and equilibrium of forces were ensured during the test, and the results follow the trends of numerical simulations of the entire structure's predicted behaviour. The observed differences with the reference curves must be put into perspective. The reference curves, even corrected with the measured temperature and measured strength of the specimen's steel, were calculated by making numerous assumptions about the behaviour of the steel and the specimen's geometric imperfections. Only the trend and the orders of magnitude must be considered. The developed virtual HFT tool is a powerful instrument to evaluate the efficiency, stability, and the effect of delays and experimental error and seems to be essential for preparing a real hybrid fire test.

Nevertheless, some limitations remain. First, the method is based on the hypothesis of decoupled DOFs, which may be questionable despite proving successful in the particular case treated in this project. This hypothesis considerably simplifies the controller's design as the gain matrices are diagonal. A research perspective is to explore the use of a non-diagonal gain matrix by building these matrices as real flexibility matrices. Another important limitation is the use of linear control; constant gain matrices do not consider the degrading physical stiffness of the PS and may result in less efficient controllers and overshoots. Adaptive control and learning gains are two avenues of investigation in further research. Additionally, the use of electric actuators makes the test easier and ensure stability because they are inherently linear systems. As the load capacity is to date limited for these jacks, the use of hydraulic actuators is therefore unavoidable for large-scale tests and must be the subject of specific research. Finally, considering a dynamic equation of movements in the controller's design may be required to follow the behaviour of the PS in the last moments of the test just before failure.

Acknowledgements

This work was supported by the National Fund for Scientific Research Belgium under Grant No. 31297790. The authors are grateful to the members of the Fire Laboratory of the University of Liege who built the experimental setup and provided help with the data acquisition system. They also thank the members of the Laboratory for Materials and Structures who helped cut the steel specimen and drill steel plates.

References

1. Hakuno M, Shidawara M, Hara T (1969) Dynamic destructive test of a cantilever beam controlled by an analog-computer. Proceedings of the Japan society of civil engineers, Japan society of civil engineers, pp 1–9
2. Korzen M, Magonette G, Buchet P (1998) Mechanical loading of columns in fire tests by means of the substructuring method. In: Proceedings of the Eighth interflam conference, Edinburgh (United Kingdom), pp 911–914
3. Robert F, Rimlinger S, Collignon C (2010) Structure fire resistance: a joint approach between modelling and full scale testing (substructuring system). 3rd fib International Congress
4. Mostafaei H (2013) Hybrid fire testing for assessing performance of structures in fire—application. Fire Saf J 56:30–38
5. Franssen J-M, Gernay T (2017) Modeling structures in fire with SAFIR: theoretical background and capabilities. J Struct Fire Eng 8:300–323
6. Pinoteau N, Pham DT, Nguyen HH, Mège R (2020) Development of hybrid fire testing by real-time subdivision of physical and numerical substructures. J Struct Fire Eng 11(4):481–497. https://doi.org/10.1108/JSFE-07-2019-0026
7. Sauca A, Gernay T, Robert F, Tondini N, Franssen J-M (2018) Hybrid fire testing: discussion on stability and implementation of a new method in a virtual environment. J Struct Fire Eng . https://doi.org/10.1108/JSFE-01-2017-0017
8. Whyte CA, Mackie KR, Stojadinovic B (2016) Hybrid simulation of thermomechanical structural response. J Struct Eng 142:04015107-1–04015107-11
9. Schulthess P, Neuenschwander M, Mosalam KM, Knobloch M (2020) A computationally rigorous approach to hybrid fire testing. Comput Struct 238:106301
10. Grolimund R (2019) Consolidated fire analysis - towards coupled numerical-experimental analysis of fire-exposed structures with stability problems. *École polytechnique fédérale de Zurich, Dissertation*
11. Wang X, Kim RE, Kwon O-S, Yeo I (2018) Hybrid simulation method for a structure subjected to fire and its application to a steel frame. J Struct Eng 144(8):04018118
12. Menari M, Wang X, Mahmoud H, Kwon O (2020) Response of a structure subjected to fire following an earthquake event. ASCE J Struct Eng 146(1):04019182
13. Abbiati G, Covi P, Tondini N, Bursi OS, Stojadinović B (2020) A real-time hybrid fire simulation method based on dynamic relaxation and partitioned time integration. J Eng Mech 146(9):04020104
14. Sauca A, Mortensen N, Drustrup A, Abbiati G (2021) Experimental validation of a hybrid fire testing framework based on dynamic relaxation. Fire Saf J 121:103315. https://doi.org/10.1016/j.firesaf.2021.103315

15. Tsokanas N, Abbiati G, Kanellopoulos K, Stojadinović B (2021) Multi-axial hybrid fire testing based on dynamic relaxation. Fire Saf J 126:103468. https://doi.org/10.1016/j.firesaf.2021.103468
16. Quershi RK (2021) Evaluation of steel columns under fire: real-time hybrid testing and reliability assessment. State University of New York at Buffalo, Dissertation
17. Mergny E, Drion G, Franssen J-M (2020) Stability in hybrid fire testing using PI control. Exp Tech 44(6):687–699
18. Sauca A (2017) Development and implementation of a methodology for hybrid fire testing applied to concrete structures with elastic boundary conditions (Dissertation). Liege University
19. Shing PB, Mahin SA (1983) Experimental error propagation in pseudodynamictesting. Report UCB/EERC-83/12, Berkeley: Earthquake Engineering Research Center, University of California
20. Urthale Y, Reddy JN (2005) Communications in numerical methods in engineering. pp 553–570
21. Mergny E (2021) Multi-degree-of-freedom hybrid fire testing in a non-linear environment. Liege University, Dissertation
22. BIPM, IEC, IFCC, ILAC, ISO, IUPAC, IUPAP and OIML (2008) Guide to the expression of uncertainty in measurement. JCGM 100 (GUM 1995 with minor corrections)